Force-Induced Lysozyme—HyHEL5 Antibody Dissociation and Its Analysis by Means of a Cooperative Binding Model

Stefan Katletz,[†] Cordula Stroh,[‡] Christian Rankl,[¶] Urbaan M. Titulaer,[†] and Peter Hinterdorfer[‡§*]
[†]Institute for Theoretical Physics, [‡]Institute for Biophysics, and [§]Christian Doppler Laboratory for Nanoscopic Methods in Biophysics, Johannes Kepler University of Linz, Linz, Austria; and [¶]Agilent Technologies-Austria, Linz, Austria

ABSTRACT Dynamic force spectroscopy probes the kinetic properties of molecules interacting with each other such as antibody-antigen, receptor-ligand, etc. In this article, a statistical model for the dissociation of such cooperative systems is presented. The partner molecules are assumed to be linked by a number of relatively weak bonds that can be grouped together into cooperative units. Single bonds are assumed to open and close statistically. Our model was used to analyze molecular recognition experiments of single receptor-ligand pairs in which the two molecules are brought into contact using an atomic force microscope, which leads to the formation of a strong and specific bond. Then a prescribed time-dependent force is applied to the complex and the statistical distribution of forces needed to pull the molecules completely apart is measured. This quantity is also calculated from our model. Furthermore, its dependence on the model parameters, such as binding free energy, number of bonds and groups, number of cooperative elementary bonds and degree of cooperativity within a group, influence of the force on the binding free energy, and the rate of change of the pulling force, is determined.

INTRODUCTION

Molecular interactions play an important role in biology. Such interactions are widely probed by single-molecule pulling experiments using atomic force microscopes, biomembrane force probes, or optical tweezers. For this, an anchored molecule is attached to a pulling spring via a linker molecule. The pulling spring is then retracted from the anchored molecule, while monitoring the force acting on the spring, resulting in characteristic force traces. The mechanical stress induced by the spring leads to a molecular transition such as dissociation of the molecular complex (1–3) or unfolding of a protein (4,5).

Various attempts have been made to interpret force traces of single-molecule pulling experiments and to obtain information from the unbinding force probability distribution functions (PDFs). One way to derive equilibrium quantities, e.g., binding free energy, is based on a remarkable theory by Jarzynski (6,7) and was successfully applied on unfolding experiments (8,9). A more classical treatment of the problem uses Kramers' (10) transition state theory (11–13). It allows one to reconstruct an equivalent free energy profile along a one-dimensional reaction pathway between the two reacting molecules (14–16) and to obtain kinetic dissociation rates. Several refinements have been proposed to this simple model. Dudko et al. (17) and Hummer and Szabo (18) assumed a linear-cubic and a quadratic cusp form of the interaction potential, respectively. This allowed us to obtain the height of the energy barrier in addition to the parameters obtained by the Evans model. Later, Dudko et al. (19) found a unified description where an additional parameter ν indicated the actual shape of the potential—allowing us to fit the actual shape of the potential ($\nu = 2/3$ and 1/2, corresponds to linear-cubic and quadratic form, respectively). In contrast to that, Raible et al. (20) assumed that in force spectroscopy the chemical bonds of the interaction complex shows a heterogeneity, leading to a dispersion of the effective dissociation length.

In this work we introduce a model using physically meaningful parameters that are in principle accessible through complementary experiments, e.g., by x-ray crystallography (21), molecular dynamics (MD) simulations (22,23), and point mutations with alanine screening (24). The model is an extension of previous work (25) into which finite cooperativity effects are incorporated. It is reminiscent of the Glauber kinetic Ising model (26), which has been used to describe the conformational transition of DNA (27). It was also inspired by the work of Montroll and Shuler (28) on the multiphoton dissociation of a diatomic molecule (in fact a discretized version of the Kramers theory) but uses a new interpretation of the energy levels. A statistical treatment like in Schwarz (29) cannot be used because of the finiteness of the Ising chain and possible boundary effects.

MATERIALS AND METHODS

Conjugation of antibody (HyHEL5) directed against lysozyme to AFM tips was performed using a flexible poly(ethylene glycol) (PEG) cross-linker as described before (30).

For force spectroscopy, a dense lysozyme layer was produced by adsorbing 10–20 μg/mL lysozyme in 1 mM NaCl (neutral pH) to freshly cleaved mica. After 15 min waiting, the sample was washed using 1 mM NaCl and finally phosphate-buffered saline.

We used a Macmode PicoSPM magnetically driven dynamic force microscope (Molecular Imaging, Phoenix, AZ) which, for force spectroscopy, was connected to a Nanoscope IIIa controller (Digital Instruments, Santa Barbara, CA). For the detection of antibody-antigen recognition, force-distance cycles were performed using antibody-coated cantilevers (cantilevers from

Submitted January 6, 2010, and accepted for publication March 29, 2010.

*Correspondence: peter.hinterdorfer@jku.at

Editor: Gerhard Hummer.

0006-3495/10/07/0323/10 $2.00

doi: 10.1016/j.bpj.2010.03.060

Veeco Instruments, Plainview, NY) with 0.01–0.03 N/m nominal spring constants in the conventional contact force spectroscopy mode. The vertical piezo-movement was 50–150 nm at sweep rates from 1 to 10 Hz. For quantification of forces and force velocities, spring constants of cantilevers were determined with the thermal noise method (31,32) and yielded spring constants of 0.009–0.034 N/m depending on the cantilever. Analysis of force distance cycles was performed using MATLAB (The MathWorks, Natick, MA) as previously described (33). For blocking of the antibody-antigen recognition, 3 μL HyHEL5 antibody was added to 197 μL phosphate-buffered saline on the lysozyme-coated mica sheets, resulting in a concentration of ~100 μg/mL. After waiting for 20–30 min, force-distance cycles were again recorded, indicating the specificity of the binding between the antibody on the tip and the lysozyme on the mica.

The functionality of lysozyme was tested with an enzyme immunoassay (as described in (30)).

EXPERIMENTAL RESULTS OF LYSOZYME AND HYHEL5 ANTIBODY INTERACTION

In high-sensitivity AFM measurements, small spring constants of the cantilevers must be chosen to measure forces down to the 10 pN-range, as they are normally obtained for single antibody-antigen-interaction (1,34,35). As these forces depend on the loading rate used for retracting the cantilever from the surface (11,15,23,36–39), we can obtain information about the dynamics of the unbinding process of ligand and receptor.

Interaction forces are measured by performing force-distance cycles. When the cantilever is first brought toward the surface, the initial lack of bending of the cantilever is measured, and the deflection angle is almost zero. Repulsive tip-sample interaction bends the cantilever upwards in the contact region, resulting in a positive change of the deflection angle. The quantity Δz, the measured deflection, is directly proportional to the interaction force $f = k \times \Delta z$ (Hooke's law), where k is the spring constant of the cantilever. Subsequent retraction first results in relaxation of the repulsive forces in the contact region (see Fig. 1, 0–10 nm). If binding between the HyHEL5 antibody on the tip and the lysozyme adsorbed to mica took place, continued retraction of the cantilever will bend the cantilever downwards, caused by the attractive pulling force developed during nonlinear stretching of the PEG-crosslinker (40) (see Fig. 1, 10–30 nm). If the tip is retracted further, the antibody will finally unbind from its antigen at a distinct critical force, termed the unbinding force f_u. Zero deflection is reached again and no more bending of the cantilever is measured during further retraction. If no binding between antibody and antigen is measured, no downward bending is observed.

Repeating such force-distance cycle measurements yielded a distribution of rupture forces (see Fig. 2). The origin of this distribution is based on the fact that the single-molecule interaction of lysozyme and HyHEL5 antibody is subject to thermal fluctuations. A second consequence of the stochastic nature of the rupture process is that the distribution of unbinding forces depends on the rate of change of the applied force (i.e., loading rate) (Fig. 2).

To calculate the loading rate, one should also know the elastic response of the PEG-molecule (40), which was stretched in order to unbind antibody and antigen. The spring constant k_{PEG} is not constant but varies with the extension of the cross-linker molecule. For calculating k_{PEG}, the wormlike chain model was used, which describes a polymer as a continuous string with a contour length L_0 and a statistically segmented or persistence length L_p that reflects the flexibility of the polymer (41). We shall approximate the exact result by (42)

$$F = W_{lc}(z) = \frac{k_{\mathrm{B}}T}{L_p}\left[\frac{1}{4(1 - z/L_0)^2} - \frac{1}{4} + \frac{z}{L_0}\right]. \quad (1)$$

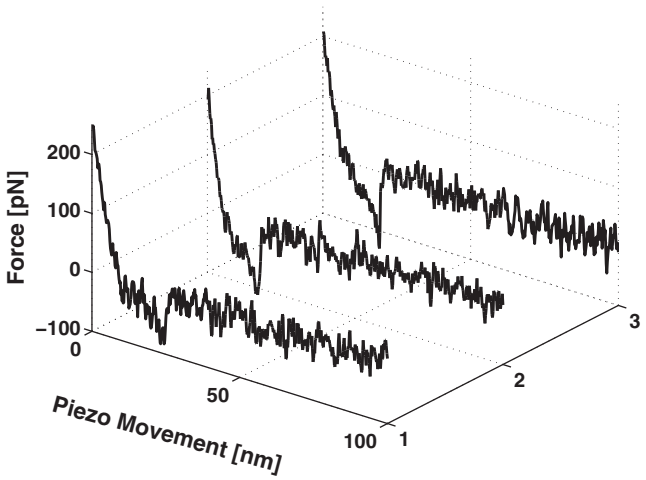

FIGURE 1 A set of typical retraction curves showing unbinding events of lysozyme-HyHEL5 antibody.

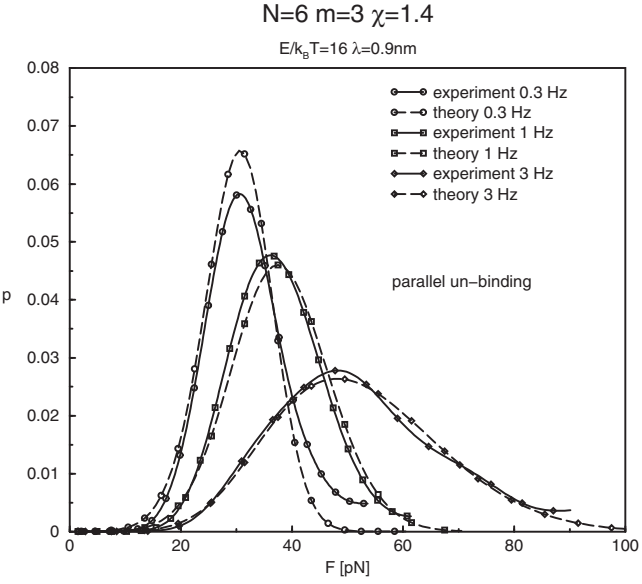

FIGURE 2 Distribution of rupture forces for various pulling frequencies. Experimental (*solid lines*) and theoretical (*dashed*) curves for the parallel unbinding model taking into account spacer effects.

In this formula, the contribution of the cantilever still has to be included. The displacement x of the piezo, on which the cantilever is mounted, and the extension of the polymer z are related by $x = z + F/k$. Then we can calculate the loading rate by

$$\frac{dF}{dt} = \frac{dF}{dx} \times v = \frac{1}{\left(W_{lc}^{-1}(F)\right)' + \frac{1}{k}} \times v, \quad (2)$$

where W_{lc}^{-1} is the inverse function of W_{lc}.

The stretching parts of the retrace of these force-distance cycles that showed unbinding events were fitted with Eq. 1 and the contour and persistence lengths were obtained. Furthermore, the first derivative dF/dz of the wormlike chain model gives the spring constant k_{PEG} depending on the extension z of the PEG molecule. Because rupture takes place at a certain extension z_R, we took the mean value of these unbinding lengths for every cantilever retraction velocity and used it for calculating k_{PEG}. Using Eq. 2, we determined loading rates from 0.2 to 5.8 nN/s.

The binding probabilities were found to correlate with the loading rates, resulting in lower binding probabilities for higher loading rates. After calibration, measured unbinding forces f_u were plotted in probability density functions (PDFs), depending on the loading rate as shown in Fig. 2 (*solid lines*). Every PDF was fitted with a Gaussian function, yielding the most likely unbinding force (maximum of distribution) and the standard deviation of it. Both were used for the force-force velocity plot, which is shown in Fig. 3 for all cantilevers used. As expected from an earlier description for force spectroscopy experiments (11), a logarithmic dependence of the maximum of the unbinding force on the loading rate was observed. In addition, the width of the distribution of unbinding force is increased with higher unbinding forces. This is in contradiction with the theoretical framework of Evans and Ritchie (11), which predicts that the width is constant with varying loading rates.

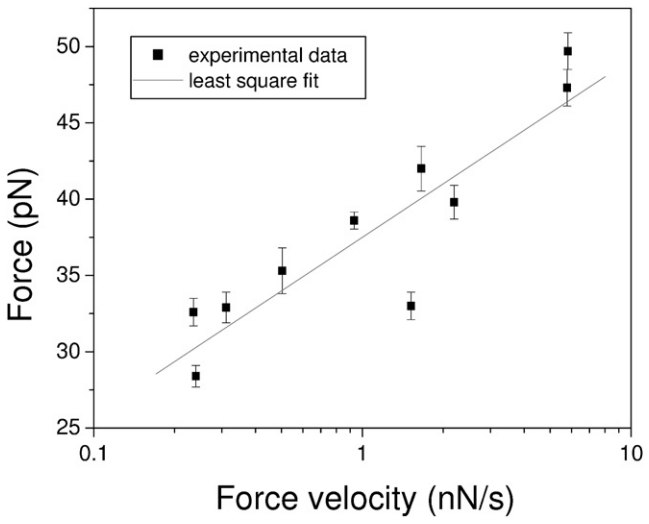

FIGURE 3 Unbinding force depends logarithmically on force velocity.

THEORY

Distribution of unbinding forces

For irreversible unbinding under the influence of an external force $F(t)$, the distribution of rupture forces is related to the survival probability of the binding complex $S(t)$ by (18)

$$p(F)dF = -\dot{S}(t)dt. \quad (3)$$

The survival probability is assumed to satisfy a first-order rate equation with a time-dependent rate coefficient (18)

$$\dot{S}(t) = -\frac{1}{\tau(F(t))}S(t), \quad (4)$$

where $\tau(F)$ is the dissociation time at force F.

Thus, the distribution of rupture forces is given by

$$p(F) = \frac{1}{\tau(F)\dot{F}(F)}\exp\left(-\int_0^F \frac{dF'}{\tau(F')\dot{F}(F')}\right), \quad (5)$$

where we have assumed that the force F is a monotonic function of time and its time derivative can be expressed as $\dot{F}(F)$.

It should be noted that Eq. 5 is only valid for quasistatic rupture experiments, i.e., when the external force is varied on a timescale much larger than the relaxation times of the molecules. Otherwise, memory effects have to be taken into account, i.e., the initial state of the complex has an influence and the description with a single dissociation time is wrong.

With our model, we want to show that the important quantity for the distribution of rupture forces is the dependence of τ on the external force F and not the exact time dependence of this force. Thus, a good approximation is obtained even if $\dot{F}(F)$ is replaced by a mean loading rate v_u at the most probable unbinding force f_u.

This is a direct consequence of the rather strong influence of an external potential on the dissociation time of the molecules. Based on Kramers' theory (10), the unbinding process can be treated as an escape from a metastable state over an energy barrier (12,36,43,44). As a first approximation, an external force reduces the dissociation time exponentially (45),

$$\tau = T_0\exp(-F\lambda/k_BT). \quad (6)$$

Assuming certain analytic forms for the energy well, corrections to this exponential dependence can be obtained (11,17,18).

Let us first obtain a first approximation for the expected behavior by assuming an exponential decay of the dissociation time and a linearly increasing force. Then the mean unbinding force and the variance of the distribution can be approximated by an analytic expression. The mean unbinding force obeys the same functional form as the maximum of the distribution (11,45). Let

$$\omega = \frac{kvT_0\lambda}{k_BT}$$

be a dimensionless loading rate, where k is the effective spring constant and v is the velocity of the cantilever of the AFM. T_0 is the dissociation time of the complex at equilibrium. The time-dependent external potential is then given by

$$\frac{F(t)\lambda}{k_BT} = \omega\frac{t}{T_0}.$$

With the abbreviation $y = F\lambda/k_BT$ and assuming an exponential decrease of the dissociation time with the applied force,

$$\tau = T_0\exp(-\alpha y), \tag{7}$$

we obtain for the mean rupture force

$$\langle F\rangle = \int_0^\infty p(F) \times F\mathrm{d}F, \tag{8}$$

$$= \frac{k_BT}{\lambda}\int_0^\infty \exp\left(-\int_0^y \frac{\tau_0}{\omega\tau(y')}\mathrm{d}y'\right)\mathrm{d}y, \tag{9}$$

$$= \frac{k_BT}{\alpha\lambda}\exp\left(\frac{1}{\alpha\omega}\right)\Gamma\left(0,\frac{1}{\alpha\omega}\right), \tag{10}$$

with the incomplete γ-function

$$\Gamma(a,z) = \int_z^\infty t^{a-1}e^{-t}\mathrm{d}t.$$

From Fig. 7, as seen later, we see that a typical value for the parameter is $\alpha \simeq 3$. Because $\omega \simeq 10^4$–10^5 in a typical experiment, we can approximate the incomplete γ-function for small arguments

$$\Gamma(0,x) \simeq -\gamma - \ln(x)$$

(Euler's constant $\gamma \simeq 0.577216$) and find, for the mean unbinding force, a logarithmic dependence on the pulling velocity

$$\langle F\rangle = \frac{k_BT}{\alpha\lambda}\ln(\alpha\omega), \tag{11}$$

which was also observed in our experiment (Fig. 3) and in the literature (12,43,46).

For the second moment of the probability distribution, we use the steepest descent method,

$$\langle F^2\rangle = \left(\frac{k_BT}{\alpha\lambda}\right)^2 2\exp\left(\frac{1}{\alpha\omega}\right)\int_0^\infty \exp\left(\ln x - \frac{1}{\alpha\omega}e^x\right)\mathrm{d}x, \tag{12}$$

$$\simeq \left(\frac{k_BT}{\alpha\lambda}\right)^2 2\sqrt{2\pi}x_0^{3/2}, \tag{13}$$

where x_0 is the solution of the equation

$$x_0 \times \exp(x_0) = \alpha\omega,$$

and can be approximated by

$$x_0 \simeq \ln(\alpha\omega) - \ln\ln(\alpha\omega).$$

Although the approximation of small forces made in deriving Eqs. 11 and 13 is too rough to be used for a comparison with experimental results, it is quite useful in predicting general trends.

New model for the antibody-antigen interaction

Instead of assuming a somewhat artificial analytic form for the binding potential, we start from a model inspired by the one introduced by Montroll and Shuler (47) for the dissociation of molecules.

In Fig. 4 we show how N_{tot} interactions between an antibody and antigen complex is organized into N groups of $m = N_{tot}/N$ bonds each. This idea is based on the results by Dall'Acqua et al. (48) and Li et al. (49) that show that the interaction region between lysozyme and the antibody is made up of several loops, and these define the places where the most relevant bonds are formed (21,22,50).

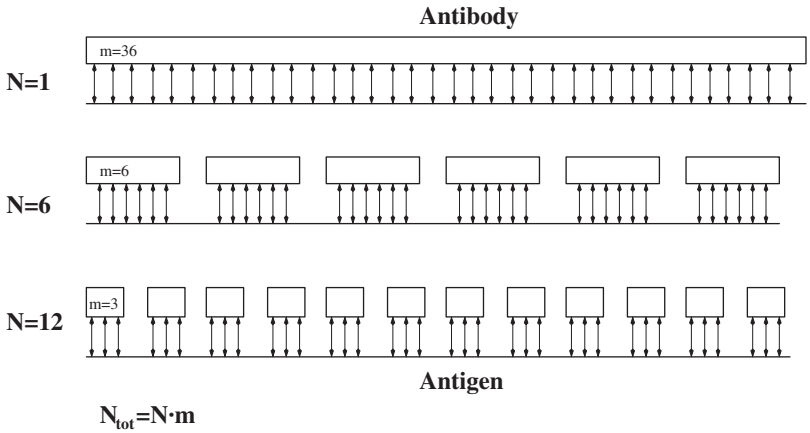

FIGURE 4 Different possibilities for the organization of bonds into groups.

Simplified noncooperative model

By dividing the molecular interactions into just N equally strong bonds or group of bonds, a discretized version of the Kramers' problem is obtained as shown in Fig. 5. The transition probabilities between the energy levels (which correspond to the number n of open bonds) up to a common prefactor are given by

$$\begin{aligned} W_{n,n+1} &= (n+1) \\ W_{n+1,n} &= (N-n)e^{-\beta\left(\Delta E - \frac{F\lambda}{N-n}\right)}, \end{aligned} \tag{14}$$

where $\Delta E = E_N/N$ is the energy per group, and F the force acting on the complex, which is assumed to be distributed equally between the remaining intact bonds. The interesting quantity of this set of differential equations is the smallest not-vanishing eigenvalue corresponding to the dissociation time of the binding (28). For not-too-large N this can be computed easily by calculating the eigenvalues of the transition matrix (see (51); however, it is important to note that the earlier thesis from that article, based on comparison with experimental data, used preliminary data, and should therefore be considered as superseded by the results in this article) or by direct integration (25).

In this simple form, i.e., for the limiting case of high cooperativity, where the bonds within one group open and close all at once, or in the low force regime, where the unbinding is much slower than the dynamics within a group, similar results are obtained as in Eqs. 13 and 16—i.e., rather narrow PDFs and only a small dependence of the width of the distributions on the pulling velocity (25).

Cooperative model

In Fig. 6 two possible unbinding pathways are depicted. In the first one, the force acts on all intact bonds simultaneously. In the second, the force is only applied on the last bond, i.e., unbinding is similar to opening a zipper, although

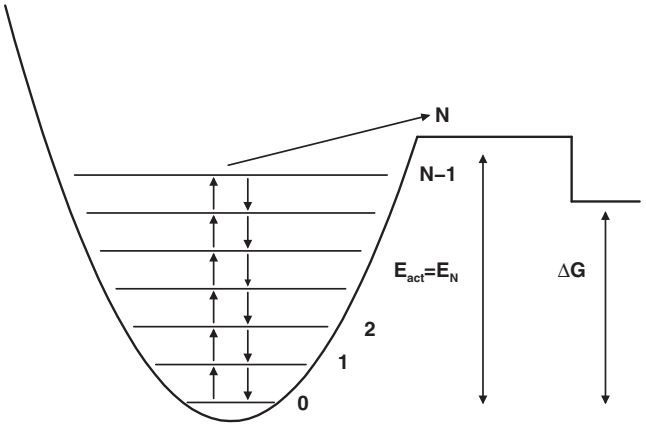

FIGURE 5 Relationship between quadratic energy landscape and number of equivalent group of bonds.

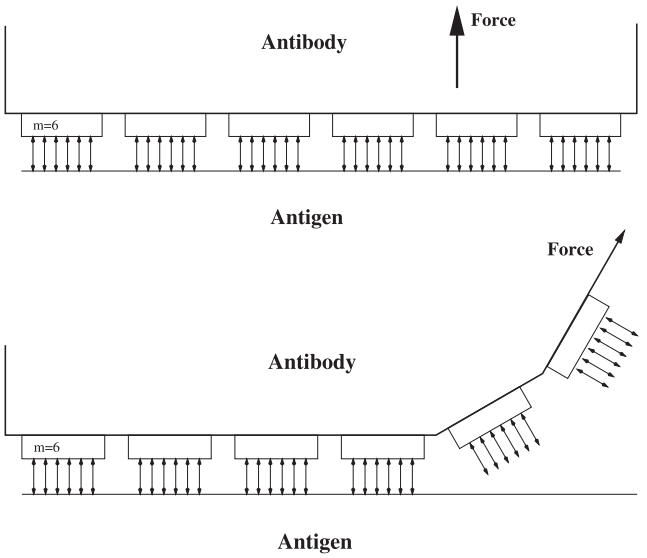

FIGURE 6 Parallel versus sequential unbinding pathway.

the other groups are still allowed to open and close statistically. We have solved both scenarios, but will only show the results of the first reaction scheme, as it seems more appropriate for the lysozyme-antibody complex (for the second, see (51); see also the note above regarding this reference).

In Eq. 14, the unbinding rate of a single group is determined by the binding energy and the applied force in an exponential factor. Now we will replace this factor with the dissociation rate of a group of m bonds that interact cooperatively.

The Hamiltonian of a linear Ising chain with nearest-neighbor interaction between m spin variables is given by

$$\mathcal{H} = -\varepsilon\sum_{i=1}^{m} b_i - \delta\sum b_i b_{i+1}, \tag{15}$$

where the variables b_i in our case take the values 0 and 1 (lattice gas interpretation) in contrast to the usual symmetric $\pm 1/2$ case. The value zero is associated with a dissociated bond whereas unity corresponds to a closed bond. There are three different possibilities for transitions in such a chain (excluding end-effects):

$$\begin{aligned} &\ldots 000\ldots \underset{r}{\overset{1}{\rightleftharpoons}} \ldots 010\ldots \\ &\ldots 100(001)\ldots \underset{r/c}{\overset{1}{\rightleftharpoons}} \ldots 110(011)\ldots \\ &\ldots 101\ldots \underset{r/c^2}{\overset{1}{\rightleftharpoons}} \ldots 111\ldots . \end{aligned} \tag{16}$$

The first possibility corresponds to a nucleation process, the second to an extension or shortening of a cluster of closed bonds, and the last to the fusion of two clusters or the breaking up into two parts. The rate constants are connected to the energy parameters in Eq. 15 by

$$r = \exp(-\beta\varepsilon),$$

$$c = \exp(\beta\delta). \tag{17}$$

It should be noted that the forward and backward rate constants are given only up to a common factor again. This factor is neglected at the moment but will have to be adjusted as discussed subsequently. The kinetics of this Ising chain is described by a master equation for all possible configurations (52):

$$\dot{x}_j = \sum_k W_{jk} x_k. \tag{18}$$

The x_j values give the probability that the chain is in state j. When the sequence $b_1 \ldots b_m$ is associated with the binary representation of j, computer modeling becomes straightforward. The value j can take values from 0 to $2^m - 1$, thus there are 2^m different configurations in all. W_{jk} is the transition probability from k to j. The only undetermined feature of the model left is how the spins at the end of the chain are treated. One can either apply periodic boundary conditions, i.e., $b_{i+m} \equiv b_i$, or open boundary conditions. In the latter case, dummy spins $b_0 = b_{m+1} = 0$ are added. Both boundary conditions give similar results, but the fitting parameters will of course differ. In the remainder of this article, we will assume the open boundary conditions.

This geometry is, of course, not intended to provide a close similarity to the actual molecular configuration. However, it corresponds roughly to a predominately linear or to a somewhat more compact grouping of the bonds.

In our experiments, a force is applied to the linkage between the two molecules. This can also be included in our model. If one assumes that the force acts equally on all intact bonds, the transition rate from state j depends on the number of closed bonds and has to be modified by the factor

$$\exp\left(\beta \frac{f\lambda}{\sum_{l=1}^{m} b_l^j}\right), \tag{19}$$

where

$$\sum\nolimits_{l=1}^{m} b_l^j$$

is the number of intact bonds in state j and f the force acting on one group. We assume that the activation free energy decreases linearly with a proportionality constant λ. This is expected to be a good approximation for not-too-strong forces. The value λ is a parameter that should be of the order of the interaction range.

The interesting quantity to be obtained from Eq. 18 is the first-passage time and its distribution, i.e., the time needed to reach the dissociated state for the first time. The calculation from Eq. 18 by direct integration or determination of the eigenvalues is impractical, because the system is stiff, i.e., the eigenvalues vary greatly in magnitude. On the other hand, this means that there is a separation of the fast relaxation timescales from the timescale on which the dissociation takes place. Hence, the first-passage time of a single group of bonds is nearly a Poisson distribution, with a single decay rate. Once a bond is broken, however, the rate constant changes due to the force redistribution, and a new Poisson process is started.

This single dissociation rate ρ_m of a single group replaces the Boltzmann factor in Eq. 14. An efficient algorithm for its calculation is included in the Appendix. Thus, the master equation for the cooperative model is given by

$$\begin{aligned} W_{n+1,n} &= (N-n) \\ W_{n-1,n} &= n\rho_m\left(r, c, \frac{F}{n}\right), \end{aligned} \tag{20}$$

where ρ_m is the unbinding rate of an Ising chain of length m subject to the force $f = F/n$.

New parameters

The connection with physical quantities is facilitated by using a different set of parameters. The total free energy of the complex E is a lower bound for the activation energy and is related to the number of cooperative units N and bonds per unit m by

$$\frac{E}{N} = -\varepsilon \times m - \delta \times (m-1). \tag{21}$$

With the introduction of a new parameter $\chi = \delta/\varepsilon$ that indicates the ratio of cooperative interaction to binding free energy, the rate constants are given by

$$r = \exp(-\beta\varepsilon) = \exp\left(-\frac{|\beta E|}{N(m + \chi m - \chi)}\right), \tag{22}$$

$$c = \exp(\beta\delta) = r^{-\chi}. \tag{23}$$

The value $\chi = \delta/\varepsilon$ as well as the interaction length λ have to be treated as fitting parameters, but they influence the mean unbinding force as well as the width of the distribution significantly.

To connect these models with the actual system under consideration, the time variable has to be rescaled such that the dissociation time without external force τ_0 corresponds to the lifetime T_0 of the complex at equilibrium, which can be determined experimentally (49).

In Fig. 7 we show the calculated behavior of the dissociation time on an external force for the parameters $E/k_BT = 20$, $m = 4$, $N = 5$, and four values of the cooperativity parameter χ. Only for small values of the external force does the dissociation time decrease exponentially, and the parameter χ controls how strong the deviation for moderate forces becomes.

In a search for the optimal parameters that give the best agreement with experiments, the total minimum of the function

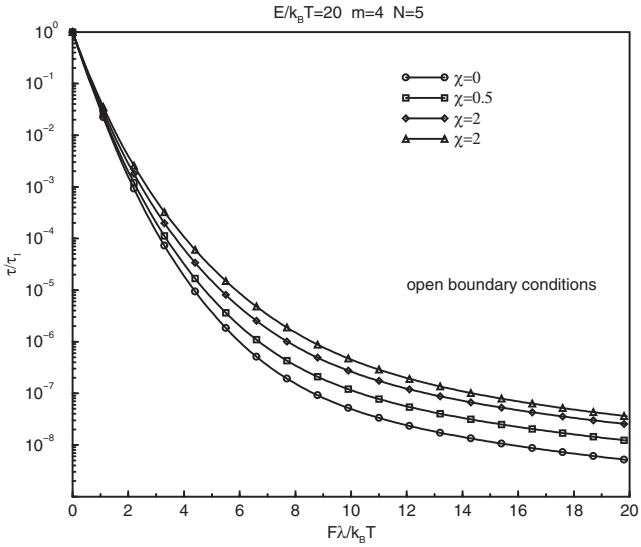

FIGURE 7 Decrease of the dissociation time as a function of the applied force.

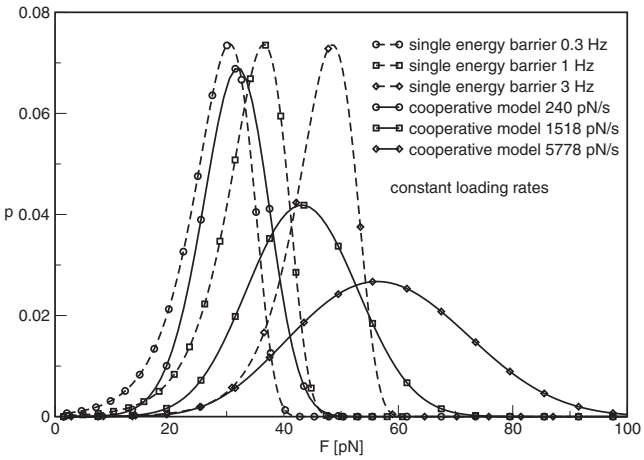

FIGURE 8 Comparison of rupture force distributions calculated with an exponential decrease of dissociation times (*dashed lines*, Eq. 6) and with the cooperative model (*solid lines*). Note that a constant loading rate was assumed for all distributions.

$$\sum_{\mathrm{f}} 10\left(F_{\max}-F_{\exp}\right)^2+\left(\sigma-\sigma_{\exp}\right)^2$$

was determined. $F_{\max}$ is the maximum of the distribution of unbinding forces and σ its standard deviation. The sum runs over all measured frequencies and the factor of 10 was included somewhat arbitrarily to give more weight to the maximum of the distribution. We confined ourselves to the PDFs for three loading rates, in which the same antibody was used. Good agreement can be obtained only for a rather narrow range of parameters: $E/k_{\mathrm{B}}T = 16$, $N = 6$, $m = 3$, $\chi = 1.4$, and $\lambda = 0.9$ nm. These parameters have been used to calculate the rupture force distributions in Fig. 2.

We think that the broadening of the PDFs with higher pulling speeds is inherent to the lysozyme-HyHEL complex and not due to other effects, e.g., the nonlinearity of the applied force over time. In Fig. 8, we also compare the results obtained from Evans' treatment (based on Bell's exponential decay of the dissociation time) with the force distributions obtained with the cooperative model for average and constant loading rates. The parameters were taken from the above fit.

DISCUSSION

The values for the score functions indicate that for the lysozyme-antibody complex the parallel unbinding pathway is more appropriate. The parallel unbinding model gives nearly perfect agreement with the experimental curves.

The introduction of cooperativity within a group of bonds allowed us to describe successfully both the shift of the maximum and the broadening of the unbinding force distributions with the loading rate. We also noted that the parameters found are in good agreement with other experimental results. From x-ray spectroscopy and MD simulations, the total number of bonds was estimated to be ~20. Our best model gives $N \times m = 18$. The estimation that ~3–5 residues contribute to the bond of a single loop of the antibody also agrees reasonably well with our results.

The parameter $x_\beta = 0.81$ nm in the simplest version of Evans' theory, determined by a fit of the maximum of the unbinding force versus the loading rate, agrees well with the parameter $\lambda = 0.9$ nm for the parallel unbinding pathway. In Fig. 8, we show the result of this Evans type theory for the unbinding probability density function (16). Clearly, the simplest Evans theory cannot reproduce the width of the distributions and their dependence on the loading rate. In this respect, it resembles an earlier version of our model, which is the limit for high χ of the model presented in this article. Because the Evans theory assumes a constant rate of change of the force, we also performed a calculation for our present model with a linearly increasing force. These results are shown in Fig. 8. We see that nonlinearity and cross-linker effects must be taken into account to obtain a really satisfactory agreement, but our model describes the qualitative dependence of the distribution shape on the loading rate much better than the simple Evans theory even for a linearly increasing force scenario.

Whether all six loops contribute equally to the overall binding is still undetermined. Measurements of kinetic rate constants of point-mutated antibodies (i.e., alanine screening) indicate that there are at least four spatially rather widely separated amino acids that play an important role in the binding. Alterations of these residues drastically reduce the dissociation time. Molecular dynamics simulations (23,53) find that all six loops play a significant role during the dissociation process. Presumably, this is also the case at the very different timescales relevant to our rupture

experiments with the AFM. Still, it is possible that the unbinding pathway is different for different force velocities, and that different rate-limiting steps are involved. Our theory assumes identical groups of bonds and therefore results in a mean number. Should experimental evidence require groups of distinct strength, it would also be possible to adapt the theory accordingly—but at the cost of introducing more parameters.

The activation energy obtained is rather low, but still close to the value obtained through BIACORE experiments. It was also found by S. J. Smith-Gill (Laboratory of Genetics, National Cancer Institute, National Institutes of Health, Bethesda, MD, personal communication, 2000) that recognition of lysozyme by an antibody is, in fact, a two-step process. An encounter state is established, which then decays into the docking state. This process takes place on a timescale that is also comparable to that of our rupture experiments. Hence, it is possible that the rupture from the energetically higher encounter state rather than from the thermodynamically preferred docking state has been determined. Therefore, the measured binding energy might still lie below the actual binding energy of our complex.

We also should admit that our model is only useful if some properties of the complex are already known, e.g., the dissociation time of the undisturbed system. Our theory does not yield absolute kinetic rates but can only estimate how kinetic rates are influenced by an external potential. Furthermore, interactions between macromolecules are dynamic processes. Reconformations take place and by applying an external force, the molecules are also deformed. The redistribution of the force over the groups that remain bound after the sequential unbinding of the different groups introduces a dynamic element into our model, but this is of course a very crude approximation to the reconformations that actually take place.

Nevertheless, we think that we have included all essential features of an antibody-antigen complex to describe the force-induced dissociation in a correct manner. It is also a statistical model that fits the measured distributions and their variations with the loading rate quite well. The number of parameters that have to be fitted is rather large, but we obtained good fits only in a very small range of the parameter space, with physically plausible values. One parameter about which independent information is hard to obtain is the cooperativity. Its introduction is essential for obtaining the right shape for the rupture force distributions at different loading rates. However, as other effects not included in our model, such as variations in the point of attachment, may also contribute to the width of the measured distributions, the numerical values obtained from our fit should be treated with caution.

CONCLUSIONS

The dynamic force spectroscopy results of lysozme-HyHEL5 antibody interaction showed that the maximum of the unbinding force distribution depends logarithmically on the applied loading rate, which is in agreement with the theory of Evans and Ritchie (11). In this article, we present a theoretical framework that is not only able to explain the loading rate dependence of the full distribution of rupture forces, but also allows us to gain detailed insights into the interaction mechanism.

Our model takes into account that the interaction between proteins consists of a large number of weak bonds, which can open and close statistically. Unbinding occurs when all weak bonds are open. In addition, we take into account that these bonds form cooperative groups, i.e., the state of the bond is influenced by its neighbor. Our new model has six parameters that need to be fitted to the experimental data:

1. The total free energy, E
2. The number of cooperative groups, N
3. The number of weak bonds per cooperative group, m
4. The bond cooperativity, χ
5. A force scale value, λ, which relates the reduction of the unbinding potential with the applied force, and
6. The kinetic off rate at zero force $k_{\mathrm{off}} = 1/\tau_0$.

In this case of the lysozyme-HyHEL5 antibody interaction we found that the number of cooperative groups and the number of bonds per groups agreed well with x-ray spectroscopy and MD simulations. The activation energy is comparable to the one found by surface plasmon resonance measurements. The λ found is close to the x_β extracted using the model of Evans and Ritchie (11).

The application of our model is not limited to antibody-antigen interactions; it could be expanded to any force spectroscopy experiments or even unfolding data.

APPENDIX

A stationary state method

This so-called trick (55) (also called flux-over-population method) has been applied for a long time (for a modern application see, e.g., (56)). The stationary solution of Eq. 18 is the state where all bonds have dissociated, i.e., $x_0 = 1$ and $x_i = 0$ for $i \neq 0$. The modification bypasses this state and leads all transitions back into the ground state. The new stationary solution will then contain a flux F through the system.

The modified transition matrices for the three-spin system are shown in Table 1. The new equation to be solved is linear and reads

$$\mathbf{W} \times \vec{x}^{\mathrm{stat}} = 0,$$

where the vector $\vec{x}$ contains the probabilities of the state $j = 1\ldots(2^m - 1)$ and is normalized by

$$\sum\nolimits_{j=1}^{2^m-1} x_j = 1.$$

TABLE 1 Stationary state matrix with open boundary conditions

Binary No.	001	010	011	100	101	110	111
State No.	1	2	3	4	5	6	7
0	r	r		r			
1	$-(r+2)$		r/c		$\boxed{r}$		
2		$-(r+2)$	r/c			r/c	
3	1	1	$-(1+2r/c)$				$\boxed{r/c}$
4				$-(r+2)$	$\boxed{r}$	r/c	
5	1			1	$-(1+2r)$		r/c^2
6		1		1		$-(1+2r/c)$	$\boxed{r/c}$
7	r	r	1	r	1	1	$-(2r/c+r/c^2)$

For periodic boundary conditions, the elements in squares are divided by c, and the diagonal elements adjusted accordingly.

Solving a set of linear equations is a stable and efficient procedure. The mean first-passage time can then be approximated as the inverse of the stationary flux,

$$\frac{1}{\tau} = \mathcal{F} = \sum\nolimits_{i=1}^{2^m-1} W_{0i} x_i^{\text{stat}}.$$

As we could show (see (51); see also the note above regarding this reference), all three methods (direct integration, eigenvalue calculation, and the stationary state method) agree quite well. The difference can be attributed to the degree of freedom one still has in choosing initial values of the probability distribution in the original model, with the thermal distribution as the natural choice.

We are indebted to the late Hansgeorg Schindler for many valuable discussions on modeling antibody-antigen kinetics. We are also much obliged to Sandra Smith-Gill for providing monoclonal HyHEL 5 antibodies. S.K. thanks Vassili Pastushenko for pointing out the stationary state method.

This work was supported by the Austrian Science Fund under projects No. 12802 MED and No. P-14549, and the Christian Doppler Society.

REFERENCES

1. Hinterdorfer, P., W. Baumgartner, …, H. Schindler. 1996. Detection and localization of individual antibody-antigen recognition events by atomic force microscopy. *Proc. Natl. Acad. Sci. USA*. 93:3477–3481.
2. Lee, G. U., L. A. Chrisey, and R. J. Colton. 1994. Direct measurement of the forces between complementary strands of DNA. *Science*. 266:771–773.
3. Moy, V. T., E.-L. Florin, and H. E. Gaub. 1994. Intermolecular forces and energies between ligands and receptors. *Science*. 266:257–259.
4. Kellermayer, M. S. Z., S. B. Smith, …, C. Bustamante. 1997. Folding-unfolding transitions in single titin molecules characterized with laser tweezers. *Science*. 276:1112–1116.
5. Rief, M., M. Gautel, …, H. E. Gaub. 1997. Reversible unfolding of individual titin immunoglobulin domains by AFM. *Science*. 276: 1109–1112.
6. Jarzynski, C. 1997. Equilibrium free-energy differences from nonequilibrium measurements: a master-equation approach. *Phys. Rev. E Stat. Phys. Plasmas Fluids Relat. Interdiscip. Topics*. 56:5018–5035.
7. Jarzynski, C. 1997. Nonequilibrium equality for free energy differences. *Phys. Rev. Lett*. 78:2690–2693.
8. Preiner, J., H. Janovjak, …, P. Hinterdorfer. 2007. Free energy of membrane protein unfolding derived from single-molecule force measurements. *Biophys. J*. 93:930–937.
9. Liphardt, J., S. Dumont, …, C. Bustamante. 2002. Equilibrium information from nonequilibrium measurements in an experimental test of Jarzynski's equality. *Science*. 296:1832–1835.
10. Kramers, H. A. 1940. Brownian motion in a field of force and the diffusion model of chemical reactions. *Physica*. 7:284–304.
11. Evans, E., and K. Ritchie. 1997. Dynamic strength of molecular adhesion bonds. *Biophys. J*. 72:1541–1555.
12. Strunz, T., K. Oroszlan, …, H. J. Güntherodt. 1999. Dynamic force spectroscopy of single DNA molecules. *Proc. Natl. Acad. Sci. USA*. 96:11277–11282.
13. Evans, E. 2001. Probing the relation between force-lifetime and chemistry in single molecular bonds. *Annu. Rev. Biophys. Biomol. Struct*. 30:105–128.
14. Balsera, M., S. Stepaniants, …, K. Schulten. 1997. Reconstructing potential energy functions from simulated force-induced unbinding processes. *Biophys. J*. 73:1281–1287.
15. Merkel, R., P. Nassoy, …, E. Evans. 1999. Energy landscapes of receptor-ligand bonds explored with dynamic force spectroscopy. *Nature*. 397:50–53.
16. Strunz, T., K. Oroszlan, …, M. Hegner. 2000. Model energy landscapes and the force-induced dissociation of ligand-receptor bonds. *Biophys. J*. 79:1206–1212.
17. Dudko, O. K., A. E. Filippov, …, M. Urbakh. 2003. Beyond the conventional description of dynamic force spectroscopy of adhesion bonds. *Proc. Natl. Acad. Sci. USA*. 100:11378–11381.
18. Hummer, G., and A. Szabo. 2003. Kinetics from nonequilibrium single-molecule pulling experiments. *Biophys. J*. 85:5–15.
19. Dudko, O. K., G. Hummer, and A. Szabo. 2006. Intrinsic rates and activation free energies from single-molecule pulling experiments. *Phys. Rev. Lett*. 96, 108191-1–4.
20. Raible, M., M. Evstigneev, …, P. Reimann. 2006. Theoretical analysis of single-molecule force spectroscopy experiments: heterogeneity of chemical bonds. *Biophys. J*. 90:3851–3864.
21. Chitarra, V., P. M. Alzari, …, R. J. Poljak. 1993. Three-dimensional structure of a heteroclitic antigen-antibody cross-reaction complex. *Proc. Natl. Acad. Sci. USA*. 90:7711–7715.
22. Heymann, B., and H. Grubmüller. 2001. Molecular dynamics force probe simulations of antibody/antigen unbinding: entropic control and nonadditivity of unbinding forces. *Biophys. J*. 81:1295–1313.
23. Grubmüller, H., B. Heymann, and P. Tavan. 1996. Ligand binding: molecular mechanics calculation of the streptavidin-biotin rupture force. *Science*. 271:997–999.
24. Wibbenmeyer, J. A., P. Schuck, …, R. C. Willson. 1999. Salt links dominate affinity of antibody HyHEL-5 for lysozyme through enthalpic contributions. *J. Biol. Chem*. 274:26838–26842.
25. Katletz, S., and U. M. Titulaer. 1999. A statistical model for antibody-antigen binding. *Cond. Matter Phys*. 2:361–368.
26. Glauber, R. J. 1963. Time-dependent statistics of the Ising model. *J. Math. Phys*. 4:294–307.

27. Pörschke, D., and M. Eigen. 1971. Co-operative non-enzymic base recognition. 3. Kinetics of the helix-coil transition of the oligoribouridylic-oligoriboadenylic acid system and of oligoriboadenylic acid alone at acidic pH. *J. Mol. Biol.* 62:361–381.

28. Montroll, E. W., and K. E. Shuler. 1958. The application of the theory of stochastic processes to chemical kinetics. *In* Advances in Chemical Physics., *Vol. 1*. John Wiley, New York.

29. Schwarz, G. 1971. General co-operative kinetics on a linear ISING lattice. *Ber. Bunsenges. Phys. Chem.* 75:40–45.

30. Stroh, C. M., A. Ebner, …, P. Hinterdorfer. 2004. Simultaneous topography and recognition imaging using force microscopy. *Biophys. J.* 87:1981–1990.

31. Hutter, J. L., and J. Bechhoefer. 1993. Calibration of atomic-force microscope tips. *Rev. Sci. Instrum.* 64:1868–1873.

32. Butt, H. J., and M. Jaschke. 1995. Calculation of thermal noise in atomic force microscopy. *Nanotechnology.* 6:1–7.

33. Baumgartner, W., P. Hinterdorfer, …, D. Drenckhahn. 2000. Cadherin interaction probed by atomic force microscopy. *Proc. Natl. Acad. Sci. USA.* 97:4005–4010.

34. Lee, G. U., D. A. Kidwell, and R. J. Colton. 1994. Sensing discrete streptavidin-biotin interactions with atomic force microscopy. *Langmuir.* 10:354–357.

35. Florin, E.-L., V. T. Moy, and H. E. Gaub. 1994. Adhesion forces between individual ligand-receptor pairs. *Science.* 264:415–417.

36. Fritz, J., A. G. Katopodis, …, D. Anselmetti. 1998. Force mediated kinetics of single P-selectin/PSGL-1 complexes observed by AFM. *Proc. Natl. Acad. Sci. USA.* 95:12283–12288.

37. Baumgartner, W., P. Hinterdorfer, and H. Schindler. 2000. Data analysis of interaction forces measured with the atomic force microscope. *Ultramicroscopy.* 82:85–95.

38. Kienberger, F., G. Kada, …, P. Hinterdorfer. 2000. Recognition force spectroscopy studies of the NTA-His_6 bond. *Single Mol.* 1:59–65.

39. Schwesinger, F., R. Ros, …, A. Pluckthun. 2000. Unbinding forces of single antibody-antigen complexes correlate with their thermal dissociation rates. *Proc. Natl. Acad. Sci. USA.* 97:9972–9977.

40. Kienberger, F., V. P. Pastushenko, …, P. Hinterdorfer. 2000. Static and dynamical properties of single poly(ethylene glycol) molecules investigated by force spectroscopy. *Single Mol.* 1:123–128.

41. Bouchiat, C., M. D. Wang, …, V. Croquette. 1999. Estimating the persistence length of a worm-like chain molecule from force-extension measurements. *Biophys. J.* 76:409–413.

42. Bustamante, C., J. F. Marko, …, S. Smith. 1994. Entropic elasticity of λ-phage DNA. *Science.* 265:1599–1600.

43. Evans, E., and K. Ritchie. 1999. Strength of a weak bond connecting flexible polymer chains. *Biophys. J.* 76:2439–2447.

44. Raab, A., W. Han, …, P. Hinterdorfer. 1997. Antibody recognition imaging by atomic force microscopy. *Nat. Biotechnol.* 17:902–905.

45. Bell, G. I. 1978. Models for the specific adhesion of cells to cells. *Science.* 200:618–627.

46. Baumgartner, W., H. J. Gruber, …, D. Drenckhahn. 2000. Affinity of *trans*-interacting VE-cadherin determined by atomic force microscopy. *Single Mol.* 1:119–122.

47. Montroll, E. W., and K. E. Shuler. 1957. Studies in nonequilibrium rate processes. I. The relaxation of a system of harmonic oscillators. *J. Chem. Phys.* 26:454–464.

48. Dall'Acqua, W., E. R. Goldman, …, R. A. Mariuzza. 1998. A mutational analysis of binding interactions in an antigen-antibody protein-protein complex. *Biochemistry.* 37:7981–7991.

49. Li, Y., H. Li, …, R. A. Mariuzza. 2003. X-ray snapshots of the maturation of an antibody response to a protein antigen. *Nat. Struct. Biol.* 10:482–488.

50. Shick, K. A., K. A. Xavier, …, R. C. Willson. 1997. Association of the anti-hen egg lysozyme antibody HyHEL-5 with avian species variant and mutant lysozymes. *Biochim. Biophys. Acta.* 1340:205–214.

51. Katletz, S. 2002. A statistical treatment of the dissociation of cooperative systems: application to the antibody-antigen system. PhD thesis, Johannes Kepler University-Linz, Linz, Austria. http://www.jku.at/fak/TNF/theophys/group/kat/diss/diss.html

52. van Kampen, N. G. 1981. Stochastic Processes in Physics and Chemistry. North-Holland Physics Publishing, Amsterdam, The Netherlands.

53. Izrailev, S., S. Stepaniants, …, K. Schulten. 1997. Molecular dynamics study of unbinding of the avidin-biotin complex. *Biophys. J.* 72: 1568–1581.

54. Reference deleted in proof.

55. Farkas, L. 1927. Nucleation in supersaturated vapors. [Keimbildungsgeschwindigkeit in übersättigten Dämpfen]. *Z. Phys. Chem.* 125: 236–242.

56. Pastushenko, V. F., Y. A. Chizmadzhev, and V. B. Arakelyan. 1979. Electrical breakdown of bilayer lipid membranes. II. Calculation of the membrane lifetime in the steady-state diffusion approximation. *Bioelectrochem. Bioenerg.* 6:53–62.